AGU PUBLICATIONS

JGR

Journal of Geophysical Research: Solid Earth

RESEARCH ARTICLE
10.1002/2014JB010943

Key Points:
- Study of stress drops of small earthquakes to assess the megathrust event
- Stress drop increases with depth between 30 and 60 km in the Tohoku-oki area
- Miyagi-oki high stress drop zone may have been a barrier for the main shock rupture

Supporting Information:
- Readme
- Table S1

Correspondence to:
T. Uchide,
t.uchide@aist.go.jp

Citation:
Uchide, T., P. M. Shearer, and K. Imanishi (2014), Stress drop variations among small earthquakes before the 2011 Tohoku-oki, Japan, earthquake and implications for the main shock, *J. Geophys. Res. Solid Earth*, *119*, 7164–7174, doi:10.1002/2014JB010943.

Received 6 JAN 2014
Accepted 22 AUG 2014
Accepted article online 28 AUG 2014
Published online 22 SEP 2014

Stress drop variations among small earthquakes before the 2011 Tohoku-oki, Japan, earthquake and implications for the main shock

Takahiko Uchide[1], Peter M. Shearer[2], and Kazutoshi Imanishi[1]

[1]Geological Survey of Japan, National Institute of Advanced Industrial Science and Technology (AIST), Tsukuba, Ibaraki, Japan, [2]Institute of Geophysics and Planetary Physics, Scripps Institution of Oceanography, University of California, San Diego, La Jolla, California, USA

Abstract It is important to assess the likely rupture characteristics of future megathrust earthquakes. One approach is to study the spatiotemporal variation of geophysical properties in active subduction zones. We explore this idea by examining stress drops of 1563 small earthquakes (M_w 3.0–4.5) shallower than 80 km in the Tohoku-oki region before the 2011 Tohoku-oki earthquake. Although individual stress drop estimates exhibit considerable scatter, we find a strong increase in stress drop with depth between 30 km and 60 km, whereas stress drops for shallower and deeper events, respectively, are nearly constant. We also identify lateral variations in stress drop along strike. Higher-than-average stress drops are found in East Aomori-oki and Miyagi-oki, whereas Sanriku-oki is a moderate stress drop area. The high stress drop zone in Miyagi-oki is located just south of the large slip area of the 2011 Tohoku-oki earthquake, and possibly acted as a barrier to further rupture propagation during the event. In addition, the frequency dependence of the seismic radiation observed during the main shock, with proportionally higher frequencies coming from the deeper parts of the fault, mimics the depth dependence we see in small earthquakes in the same region. These results imply that smaller pre-main shock earthquakes can provide insight into the fault properties and consequent rupture processes of future megathrust earthquakes.

1. Introduction

The 2011 Tohoku-oki earthquake (M_w 9.0) striking Northeast Japan had a huge human and scientific impact. Seismologists have used the unprecedented quantity and quality of near- and far-field data to understand this earthquake and apply its lessons to other megathrust earthquakes. Thanks to a number of slip inversions [e.g., *Ide et al.*, 2011; *Koketsu et al.*, 2011; *Lay et al.*, 2011; *Ozawa et al.*, 2011; *Shao et al.*, 2011; *Suzuki et al.*, 2011; *Yagi and Fukahata*, 2011; *Evans and Meade*, 2012; *Iinuma et al.*, 2012; *Uchide*, 2013] and backprojection studies [e.g., *Koper et al.*, 2011; *Meng et al.*, 2011; *Simons et al.*, 2011; *Wang and Mori*, 2011; *Yao et al.*, 2011; *Kiser and Ishii*, 2012; *Maercklin et al.*, 2012; *Roten et al.*, 2012; *Yao et al.*, 2012], we have good constraints on the coseismic process of the 2011 Tohoku-oki earthquake. A highlight of the findings is at least 30 m of fault slip near the Japan Trench, although the backprojection images from high-frequency teleseismic seismograms (e.g., 0.1–1 Hz) indicate that the seismic radiation at high frequencies came from areas close to Honshu Island, i.e., the deeper portion of the plate interface.

Additional constraints on the 2011 Tohoku-oki earthquake include geological studies to reveal the long-term history of earthquakes and geophysical studies to investigate interseismic and coseismic mechanisms. The Japan Trench Fast Drilling Project examined the rocks of the shallow plate interface in the Tohoku-oki region from the fault core obtained by seafloor drilling [*Chester et al.*, 2013] and found low coseismic friction from laboratory experiments [*Ujiie et al.*, 2013] and in situ temperature measurements [*Fulton et al.*, 2013]. *Lin et al.* [2013] investigated borehole breakouts to infer drastic stress changes in the frontal prism caused by a nearly complete stress drop in the main shock. The geophysical studies examine parameters resolved on and around the plate interface. Reports now constrain the coupling rate on the plate interface [*Uchida and Matsuzawa*, 2011, 2013], resolve a low *P* wave velocity anomaly above the plate interface [*Zhao et al.*, 2011], and suggest a decade-scale decrease of Gutenberg-Richter *b* value in the large slip area of the 2011 Tohoku-oki earthquake [*Nanjo et al.*, 2012].

The stress drops of small earthquakes provide geophysical information on the fault properties in various ways. In this paper, we consider stress drops of small earthquakes, defined as the average change in shear

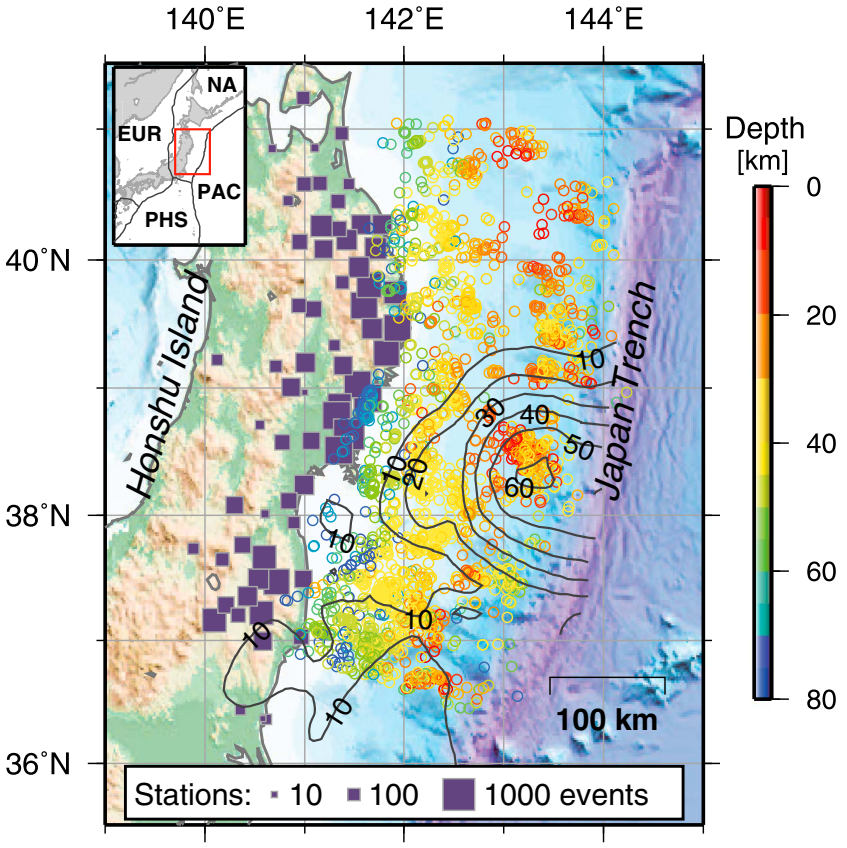

Figure 1. Map of the study area. The circles are epicenters of the earthquakes we study, and their colors indicate depth. The purple squares are the locations of the seismic stations we use and their areas are proportional to the number of events recorded. The black contours are every 10 m for the slip distribution of the 2011 Tohoku-oki earthquake [*Uchide*, 2013].

stress over the rupture area based on a circular crack model. A number of studies [e.g., *Kanamori and Anderson*, 1975] have found that the stress drops of intraplate earthquakes are larger than those of interplate earthquakes. Analyses of seismic networks enable us to investigate the spatial variations of stress drops in specific regions in order to understand the details of fault properties. *Hardebeck and Aron* [2009] suggested, based on a stress drop analysis of earthquakes on the Hayward Fault, Northern California, that stress drops of small earthquakes are correlated with the applied shear stress, but not with rock strength. They also found higher stress drops for earthquakes around a locked patch than those in creeping sections. For earthquakes around an injection well, a spatial variation of stress drops is correlated with pore pressure [*Goertz-Allmann et al.*, 2011]. On the other hand, the correlation of stress drops of aftershocks with large slip patches is still ambiguous: both positive [*Shearer et al.*, 2006; *Allmann and Shearer*, 2007; *Yamada et al.*, 2010] and negative [*Shearer et al.*, 2006; *Allmann and Shearer*, 2007] correlations have been observed.

This paper studies the spatial and temporal distribution of the stress drops of small earthquakes (M_w 3.0–4.5) in the Tohoku-oki region before the 2011 Tohoku-oki earthquake and their relationship to the rupture process of the main shock. Our analysis approach is similar to that recently applied by *Oth* [2013] to study earthquake stress drops across Japan, but we focus on the offshore Tohoku region in more detail. Stress drops in the Tohoku-oki region were studied a decade ago by *Yamashita et al.* [2004]; here we examine more recent data using the borehole seismic network, Hi-net of the National Research Institute of Earth Science and Disaster Prevention (NIED), Japan. Other relevant studies include those of moderate to large earthquakes that found that deeper earthquakes have shorter source durations relative to magnitude [*Bilek and Lay*, 1999; *Bilek et al.*, 2012] and larger stress drops [*Ye et al.*, 2013] in the Tohoku-oki region. Compared to these studies, we examine a larger number of smaller earthquakes to obtain a more detailed spatiotemporal description of stress drop variations, which will help us to resolve spatial variations in fault properties.

Table 1. List of Hi-net Stations Used in This Study

	Station Name	Latitude	Longitude	# of Events
1	N.SZGH	38.6416	141.4428	924
2	N.TOWH	38.7860	141.3254	758
3	N.KKWH	38.9207	141.6377	744
4	N.KAKH	38.5158	141.3421	735
5	N.YMDH	39.4734	141.9336	696
6	N.RZTH	39.0307	141.5320	680
7	N.KANH	39.6442	141.5977	671
8	N.MKJH	37.4703	140.7227	634
9	N.KMIH	39.2741	141.8233	614
10	N.IWZH	39.8020	141.6520	585
11	N.FSWH	38.8654	141.3512	531
12	N.HTAH	37.2169	140.5703	515
13	N.NGUH	37.1616	140.0930	491
14	N.KMAH	37.6636	140.5974	487
15	N.TROH	39.7435	141.9087	444
16	N.NHWH	40.2611	141.1709	430
17	N.KJSH	40.0861	141.7120	423
18	N.KZMH	39.9398	141.5492	369
19	N.KHEH	40.1533	141.4245	369
20	N.KASH	39.4630	141.6775	369

2. Data

Figure 1 shows the stations and events used in our study. We obtain seismograms from 151 borehole seismometers of Hi-net [*Okada et al.*, 2004] of NIED. Twenty of these stations that record the most events are listed in Table 1 and the complete station list is available in the supporting information. We choose earthquakes shallower than 80 km, over East Aomori-oki, Sanriku-oki, Miyagi-oki, and Fukushima-oki, with Japan Meteorological Agency (JMA) magnitudes (M_j) of 3.0 to 6.0, from April 2004, using Hi-net data available online, to 5:45 (UTC) 11 March 2011, 1 min before the 2011 Tohoku-oki earthquake. We limit the event depth, because we are most interested in interplate earthquakes, which will be appropriate for comparing with the 2011 Tohoku-oki earthquake. However, we initially examine all earthquakes, including intraplate events, in order to stabilize the analysis by gathering more earthquakes. We require the earthquakes to have picked *P* arrivals from the JMA Unified Earthquake Catalog at five or more stations, resulting in 3044 earthquakes for our analysis.

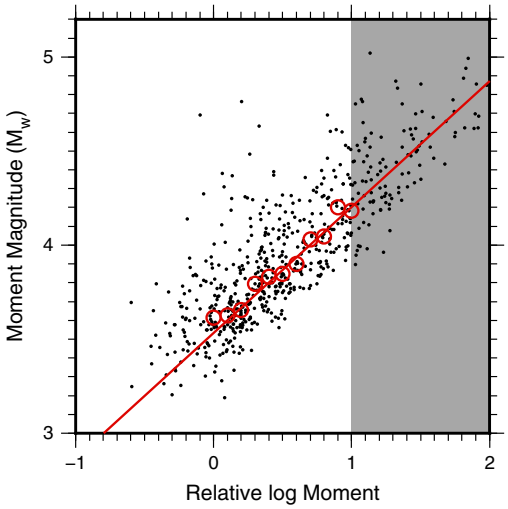

Figure 2. Comparison between relative log moment from the low-frequency average of the event terms and the moment magnitude from the NIED F-net CMT solutions. Red circles and lines are the median of the moment magnitude in 0.1-log-magnitude bins and the regression line, respectively. The root mean square of the misfit in the range between 0.0 and 1.0 of the relative log moment is 0.21. The area above unit relative log moment is shaded, because the seismic moment is poorly estimated from the 2.56 s *P* wave windows.

We use 2.56 s windows of the *P* arrival as well as a pre-*P* noise window. We require the average signal amplitude spectra in 0.5–2 Hz, 2–8 Hz, and 8–32 Hz passbands to be at least 5 times larger than the noise spectra. There are 2475 earthquakes that passed these signal-to-noise ratio criteria.

3. Method

We apply the spectral analysis method described by *Shearer et al.* [2006] to this data set. The logarithm of the observed displacement spectrum, $d_{ij}(f)$, for event i and station j is written as

$$d_{ij}(f) = e_i(f) + s_j(f) + t_{k(i,j)}(f) + r_{ij}(f), \qquad (1)$$

where e_i, s_j, $t_{k(i,j)}$, and r_{ij} are the event, station, traveltime, and residual terms, respectively. The

Table 2. Shear Wave Velocity Structure After an Average Velocity Structure [*Zhao et al*., 1992]

Depth (km)	v_s (km/s)
0–10	3.25–3.49
10–20	3.49–3.74
20–32	3.74–4.07
32–50	4.41–4.43
50–100	4.43–4.50

event term includes the relative source spectrum, the station term includes the site effect and instrument response, and the traveltime term includes the geometrical spreading and anelastic attenuation. This decomposition is done separately for each frequency.

Since the event terms only provide relative moment rate spectra, we need to calibrate them. For the low-frequency part, we calibrate them in a slightly different way than *Shearer et al*. [2006], by using the seismic moment from NIED F-net Centroid Moment Tensor (CMT) solutions. Since the NIED F-net CMT solutions are available for only 603 of the earthquakes, we obtain a regression line of the relative seismic moment to the absolute seismic moment using earthquakes with the CMT solutions, and apply the regression line for all events. The relative seismic moment is calculated from the logarithmic average of the third, fourth, and fifth lowest frequency points (i.e., 0.78 Hz, 1.17 Hz, and 1.56 Hz, respectively) of the event term spectra. We fit the relative log moment and the moment magnitude with a line with a slope of 2/3, following the definition of the moment magnitude: $M_w = (2/3)(\log_{10} M_o - 9.1)$, where M_o is the seismic moment in N m [*Kanamori*, 1977]. Plots of F-net moment versus our estimated relative moment (Figure 2) show that our relative moments are unreliable for $M_w > 4.5$ events, presumably because these large moments cannot be recovered from a 2.56 s window. We therefore exclude $M_w > 4.5$ events from further analysis. We then fit a regression line: $M_w = (2/3)\log_{10}\tilde{M}_o + 3.53$, where $\tilde{M}_o$ is the relative seismic moment. This regression line is then applied to estimate absolute moment from our relative moment estimates for all of the events (i.e., not just those with F-net moments).

For higher frequencies, we calibrate the relative source spectra by assuming that the stacked spectra in 0.2-magnitude bins follow the ω^{-2} model with a constant stress drop. The displacement spectrum, $u(f)$, is written as

$$u(f) = \frac{\Omega_0}{1 + (f/f_c)^2} \tag{2}$$

where Ω_0 is the low-frequency amplitude and f_c is the average corner frequency, which is related to the stress drop, $\Delta\sigma$, assuming a circular crack model [*Madariaga*, 1976], by

$$f_c = \frac{0.42 v_s}{(M_o/\Delta\sigma)^{1/3}}, \tag{3}$$

where v_s is the shear wave velocity, which in general will depend on the event depth. This study assumes a 1-D shear wave velocity structure (Table 2) after an average velocity structure [*Zhao et al*., 1992].

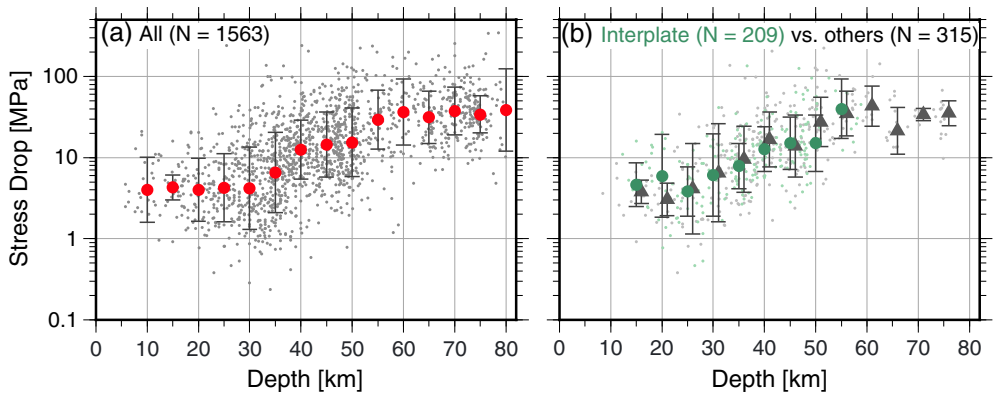

Figure 3. Estimated stress drops versus event depth. The dots and large symbols denote the stress drops of individual events and the median of the stress drops in 5 km event depth bins, respectively. (a) All results. (b) The stress drop of earthquakes with NIED F-net CMT solutions. Green and gray colors indicate the interplate and other events, respectively. We slightly shift the green and gray symbols for the median stress drop in order to avoid symbol overlap.

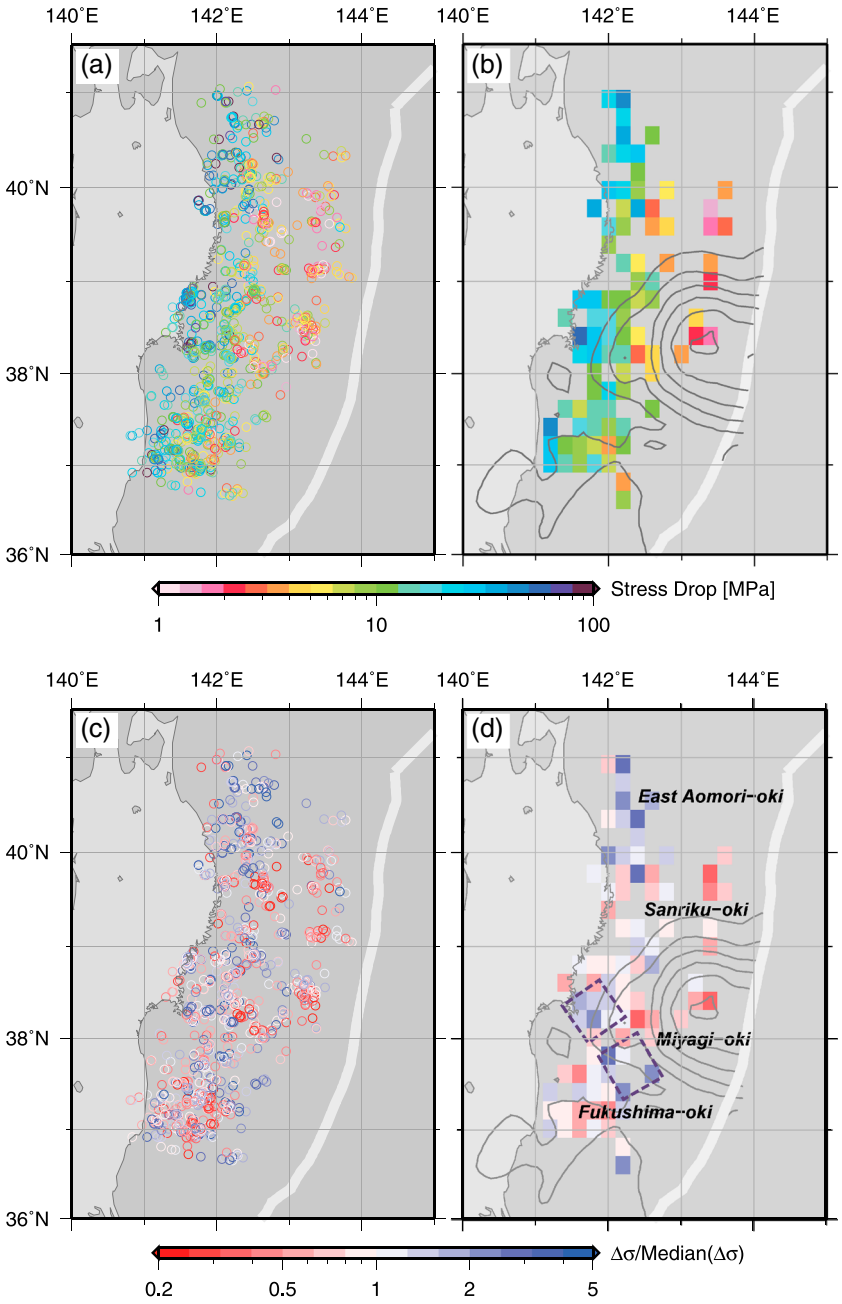

Figure 4. Spatial distribution of the stress drops of near-plate small earthquakes. (a) Stress drops of individual events. (b) Median of stress drops of small earthquakes in a 0.2° grid. Only grids with five or more events are filled. (c) Stress drop deviation, the ratio of stress drop to the median stress drop in 5 km depth bins. (d) Median of the stress drop deviation in a 0.2° grid. The 10 m contours in Figures 4b and 4d indicate the slip distribution of the 2011 Tohoku-oki earthquake [*Uchide*, 2013]. Only grids with five or more events are filled. The dashed boxes indicate the Miyagi-oki high stress drop zone.

The empirical Green's function (EGF) is then defined as the single calibration spectra, which, when subtracted from the different binned source spectra, provides the best overall fit to the constant stress drop model.

For earthquakes with estimated moment magnitudes between 3.1 and 4.4, we estimate the absolute moment rate spectra using the EGF calibration, fit their corner frequencies with the ω^{-2} model (equation (2)), and estimate stress drops by applying the circular crack model (equation (3)).

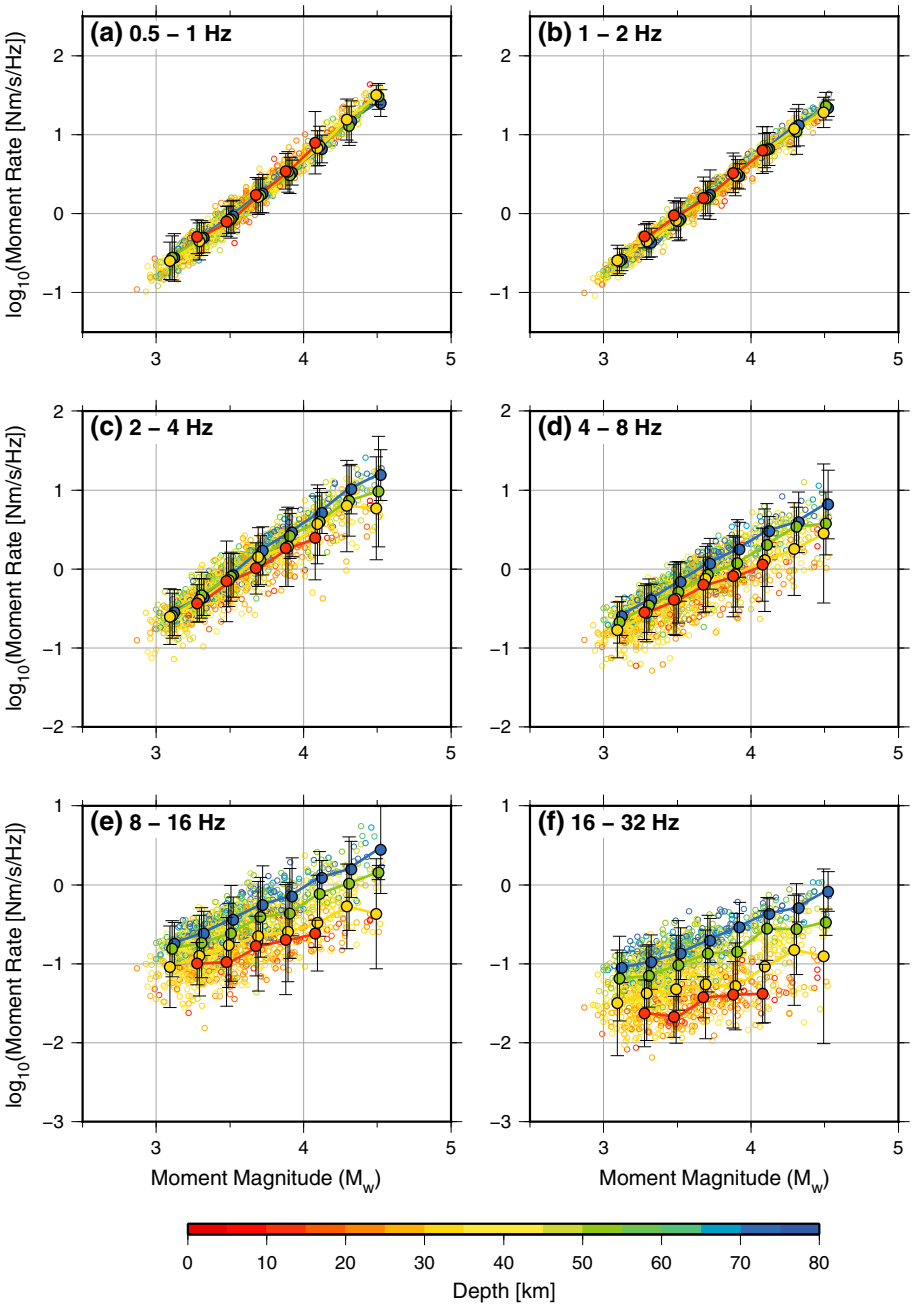

Figure 5. Depth and magnitude dependency of the frequency content of the moment rate spectra in (a) 0.5–1 Hz, (b) 1–2 Hz, (c) 2–4 Hz, (d) 4–8 Hz, (e) 8–16 Hz, and (f) 16–32 Hz. The small open circles are moment rates of individual events. The solid circles and bars indicate median values and median absolute deviations, respectively, of logarithms of the moment rate in 20 km depth and 0.2 magnitude bins.

4. Results

We succeeded in obtaining the moment rate spectra and estimated stress drops for 1563 earthquakes. In order to examine large-scale variations of the stress drops in space or time, we take the median of stress drops in bins, rather than the average, to provide representative stress drops, since the median is less affected by outliers. The most obvious spatial variation that we observe is a strong increase in median stress drop with depth between 30 km and 60 km, although large scatter is observed for single events (Figure 3a). The stress drops of earthquakes shallower than 30 km and deeper than 60 km do not show clear depth dependence.

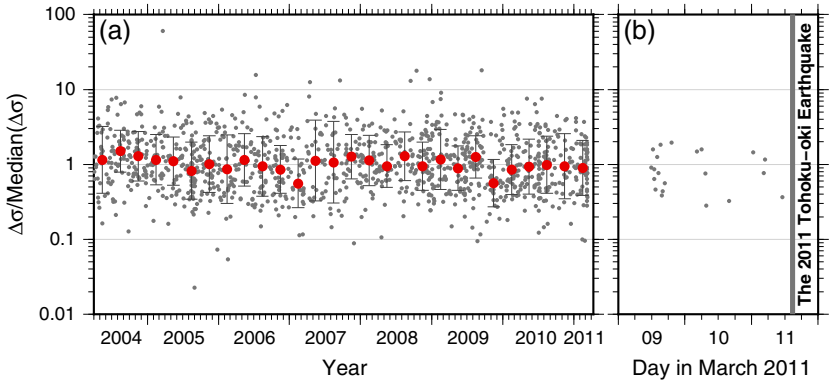

Figure 6. Normalized stress drop versus time for (a) the entire study period and (b) the 2 day foreshock period. The red circles and black bars show the medians and the median absolute deviation, respectively, of the stress drop in 3 month bins.

Note that these results do not assume a constant rupture velocity with depth; rather we have used shear velocities from the 1-D velocity-depth model (Table 2) in equation (3) for the stress drop.

Since it is difficult to distinguish interplate and other earthquakes solely from the earthquake catalog mainly because of uncertainties in the event depths, we classify interplate earthquakes both by event depth and CMT solutions. First we select 1191 "near-plate" earthquakes within 10 km from the plate interface model [*Nakajima and Hasegawa*, 2006; *Hirose et al*., 2008; *Nakajima et al*., 2009; *Kita et al*., 2010]. Then we classify the near-plate events into interplate earthquakes and off-plate events using the F-net CMT solutions that are available for 524 earthquakes of those we studied. We regard earthquakes as interplate if their focal mechanism is within 25° of Kagan's angle [*Kagan*, 1991] from pure reverse faulting on the plate interface, i.e., the strike and dip angles from the plate interface, and 90° of the rake angle. Using this criterion, which is more restrictive than that in *Asano et al*. [2011], 209 of 524 earthquakes are defined as interplate earthquakes. Since we do not see any systematic differences between the stress drops of the interplate earthquakes and the off-plate events (Figure 3b), we do not distinguish them further, but discuss the entire near-plate population as a whole. It is unclear how many of the small earthquakes we study occurred on exactly the same fault as the Tohoku-oki earthquake.

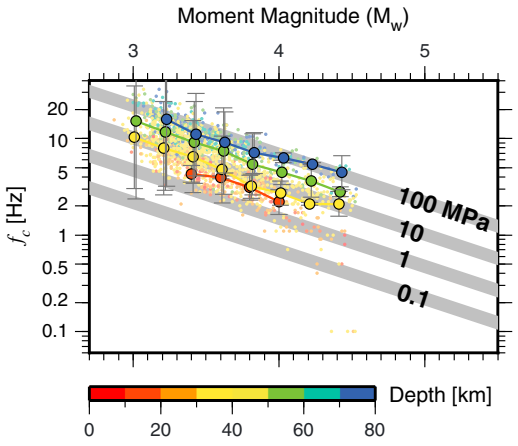

Figure 7. Corner frequencies versus moment magnitude. The small dots show the corner frequencies of individual events. The solid circles and bars indicate median values and median absolute deviation, respectively, of logarithms of corner frequencies in 20 km depth and 0.2 magnitude bins. The colors indicate the event depths. Gray belts indicate constant stress drop from equation (3) with shear wave velocities between the minimum and maximum values in Table 2, i.e., 3.25 and 4.5 km/s.

The spatial distributions of the stress drops are shown in Figure 4. Since we see a clear dependence of the median stress drop on event depth, to accentuate lateral variations at similar depths, we normalize the stress drops by the median stress drops of earthquakes in 5 km depth bins (Figures 4c and 4d). In order to clarify the large-scale variations, we take median values in 0.2° grids that contain five or more events (Figures 4b and 4d). This reveals two prominent high stress drop zones: East Aomori-oki and Miyagi-oki. In contrast, Sanriku-oki is a moderate or relatively low stress drop zone. The Miyagi-oki high stress drop zone is located on the southern rim of the large slip area of the 2011 Tohoku-oki earthquake.

The frequency content of the spectra as a function of M_w is shown in Figure 5. As expected, amplitude grows as a function of moment. At lower frequencies, the amplitudes are identical for different event depths, because they are directly related to the seismic moment. At higher frequencies, it is clear that

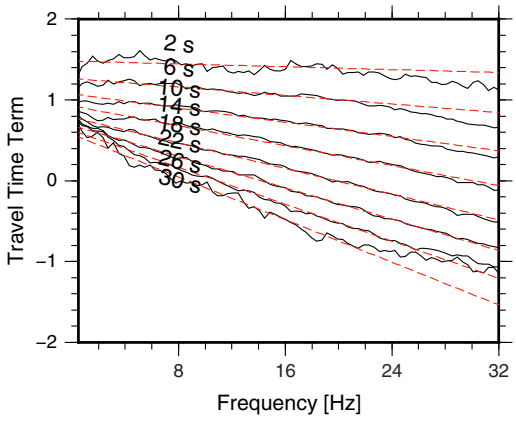

Figure 8. Traveltime terms (black) and their fits by a constant $Q_p = 620$ model (red dashed). The numbers show the *P* wave traveltimes of the traveltime terms.

the deeper earthquakes radiate more energy than the shallow earthquakes. This is also indicated by the depth dependency of the estimated stress drops, but Figure 5 is a more direct observation of the higher frequencies radiated by the deep earthquakes because it does not assume any particular source model.

The stress drop deviations do not exhibit any clear temporal trends (Figure 6), including the 2 days of foreshock activity of the 2011 Tohoku-oki earthquake (Figure 6b). The absolute value of the stress drops during the 2 day foreshock period is relatively low, but this is consistent with their shallow event depths. Finally, our data set does not show a clear deviation from magnitude-independent stress drop (Figure 7). It should be noted that there is large scatter in stress drop even among nearby events, which has been seen in other stress drop studies [e.g., *Imanishi and Ellsworth*, 2006; *Shearer et al.*, 2006]. Some of this scatter may be attributed to measurement uncertainties and errors, but it is likely that a considerable component reflects real variations in stress drop caused by heterogeneous prestress and faulting complexity.

5. Discussion

Could the apparent depth dependence of the stress drop be some kind of processing artifact, i.e., can we be sure that stress drop truly does increase with depth? One possible source of bias is the shear wave velocity. Inaccuracies in the velocity structure (Table 2) could affect the stress drop estimation, because the estimated stress drop is inversely proportional to the cube of the shear wave velocity (equation (3)). However, it is very unlikely that the shear wave velocity errors exceed 25% according to tomography studies [e.g., *Zhao et al.*, 1992]; thus, uncertainties in velocity cause stress drop errors of less than a factor of 2, much less than the observed nearly an order of magnitude increase in stress drop with depth. Therefore, it is impossible to explain the depth dependency of apparent stress drop only from possible inaccuracies of the depth-dependent shear wave velocity.

Another factor that may bias stress drop estimates is the traveltime terms, because they include a quality factor (Q) correction that affects the high-frequency falloff in the spectra. Because the station distribution is one-sided, errors in Q could introduce distance-dependent errors that could cause a depth dependence of stress drop. We evaluate the accuracy of the traveltime terms by testing whether they are consistent with a reasonable constant Q_p value. We search for the best fitting Q_p value that fits the traveltime terms over 2–30 s in traveltime and 1–16 Hz in frequency. The resulting $Q_p = 620$ value fits the traveltime terms very well (Figure 8). This Q_p value is comparable to published attenuation models [*Tsumura et al.*, 2000; *Takahashi*, 2012]. This suggests the path effect is reasonable and is not biasing the source spectral estimates.

The overall depth dependency of the stress drop was also found by prior studies [*Oth*, 2013; *Ye et al.*, 2013]. A possible contributor to the depth dependence is that the confining pressure increases with depth making faults stronger and able to store more shear stress. However, exactly how an increase in absolute stress relates to stress drop and why the stress drop change would occur mainly between 30 and 60 km depth (Figure 3) is not clear and warrants further study. The fact that the deeper earthquakes have larger stress drops is consistent with findings that the deeper earthquakes are richer in high frequencies than the shallow earthquakes (Figure 5) and have longer durations relative to magnitude [*Bilek and Lay*, 1999; *Bilek et al.*, 2012]. This is apparently similar to observations for the radiation behavior of the main shock [e.g., *Koper et al.*, 2011; *Meng et al.*, 2011; *Simons et al.*, 2011; *Wang and Mori*, 2011; *Yao et al.*, 2011; *Kiser and Ishii*, 2012; *Maercklin et al.*, 2012; *Roten et al.*, 2012; *Yao et al.*, 2012], although the origin of this depth dependence is unclear. Since high-frequency seismic waves are radiated from spatial variability in rupture velocity [e.g., *Spudich and Frazer*, 1984; *Pulido and Dalguer*, 2009; *Uchide et al.*, 2013], the depth dependency of high-frequency radiation of small earthquakes may reflect differences in the roughness of fault properties.

We suggest that the Miyagi-oki high stress drop zone located near the southern edge of the large slip area of the 2011 Tohoku-oki earthquake (the blue dashed boxes in Figure 4d) is probably relatively strong, since it has been reported that earthquakes in a locked zone tend to have larger stress drops than those in a creeping zone [*Hardebeck and Aron*, 2009]. If so, this zone possibly acted as a barrier during the 2011 Tohoku-oki earthquake. The small earthquakes have only ruptured a small part of this zone, which is likely recovering strength by healing mechanisms [e.g., *Marone*, 1998]; therefore this zone is likely still strong. On the other hand, the Sanriku-oki area shows moderate stress drops, surrounded by the East Aomori-oki and Miyagi-oki high stress drop zones, while repeating earthquakes have large stress drops [*Uchida et al*., 2012]. The seismicity there is relatively low [*Ye et al*., 2012]. This suggests relatively weak coupling and a weak fault, but the correspondence of the stress drops of small earthquakes to the slip rate over the study area [*Uchida and Matsuzawa*, 2013] is not clear.

The seismic observations, including the spatial distribution of stress drops, the anomalies of the seismic wave velocity of the hanging plate [*Zhao et al*., 2011], the plate motion inferred from repeating earthquakes [*Uchida and Matsuzawa*, 2013], and the fluctuations of the *b* value of the magnitude-frequency distribution just before the main shock [*Nanjo et al*., 2012], suggest spatial variations of fault properties and provide clues regarding likely rupture behavior during larger megathrust earthquakes, though the specific relationship of these observations to the state of the fault is still ambiguous and should be further studied by a variety of approaches.

6. Conclusions

In order to study the fault properties of the plate interface in the Tohoku-oki region and their implications for the 2011 Tohoku-oki earthquake, we investigated small earthquakes (M_w 3.0–4.5) shallower than 80 km before the 2011 Tohoku-oki earthquake. For earthquakes between 30 and 60 km of depth, stress drops inferred from source spectra increase strongly with earthquake depth, while those of shallower and deeper earthquakes do not show clear depth dependency. Stress drops of interplate and off-plate earthquakes classified using CMT solutions are not systematically different. High stress drop zones are found in East Aomori-oki and Miyagi-oki, whereas the stress drops are moderate in Sanriku-oki. The Miyagi-oki high stress drop zone is located to the south of the large slip patch of the 2011 Tohoku-oki earthquake and may have acted as a barrier for the main shock rupture. The fact that the deeper earthquakes radiate more high frequency energy is apparently similar to the frequency-dependent radiation in the 2011 Tohoku-oki earthquakes, though the physical mechanism of these observations should be further investigated. Small earthquakes provide clues to assess fault properties and the resultant rupture processes of future megathrust events.

Acknowledgments

Discussions with Yasuto Kuwahara were helpful to improve this study. The authors thank Associate Editor, Weiren Lin, and one anonymous reviewer. We used the JMA Unified Earthquake Catalog, NIED F-net CMT solutions, and seismograms from NIED Hi-net. Figures are made using Generic Mapping Tools (GMT) [*Wessel and Smith*, 1991].

References

Allmann, B. P., and P. M. Shearer (2007), Spatial and temporal stress drop variations in small earthquakes near Parkfield, California, *J. Geophys. Res.*, *112*, B04305, doi:10.1029/2006JB004395.

Asano, Y., T. Saito, Y. Ito, K. Shiomi, H. Hirose, T. Matsumoto, S. Aoi, S. Hori, and S. Sekiguchi (2011), Spatial distribution and focal mechanisms of aftershocks of the 2011 off the Pacific Coast of Tohoku Earthquake, *Earth Planets Space*, *63*, 669–673, doi:10.5047/eps.2011.06.016.

Bilek, S. L., and T. Lay (1999), Comparison of depth dependent fault zone properties in the Japan trench and Middle America trench, *Pure Appl. Geophys.*, *154*, 433–456, doi:10.1007/s000240050238.

Bilek, S. L., H. R. DeShon, and E. R. Engdahl (2012), Spatial variations in earthquake source characteristics within the 2011 M_w = 9.0 Tohoku, Japan rupture zone, *Geophys. Res. Lett.*, *39*, L09304, doi:10.1029/2012GL051399.

Chester, F. M., et al. (2013), Structure and composition of the plate-boundary slip zone for the 2011 Tohoku-Oki earthquake, *Science*, *342*, 1208–1211, doi:10.1126/science.1243719.

Evans, E. L., and B. J. Meade (2012), Geodetic imaging of coseismic slip and postseismic afterslip: Sparsity promoting methods applied to the great Tohoku earthquake, *Geophys. Res. Lett.*, *39*, L11314, doi:10.1029/2012GL051990.

Fulton, P. M., et al. (2013), Low coseismic friction on the Tohoku-Oki fault determined from temperature measurements, *Science*, *342*, 1214–1217, doi:10.1126/science.1243641.

Goertz-Allmann, B. P., A. Goertz, and S. Wiemer (2011), Stress drop variations of induced earthquakes at the Basel geothermal site, *Geophys. Res. Lett.*, *38*, L09308, doi:10.1029/2011GL047498.

Hardebeck, J. L., and A. Aron (2009), Earthquake stress drops and inferred fault strength on the Hayward fault, East San Francisco Bay, California, *Bull. Seismol. Soc. Am.*, *99*, 1801–1814, doi:10.1785/0120080242.

Hirose, F., J. Nakajima, and A. Hasegawa (2008), Three-dimensional velocity structure and configuration of the Philippine Sea slab beneath Kanto district, Central Japan, estimated by double-difference tomography [in Japanese], *Zisin J. Seismol. Soc. Jpn. 2nd Ser.*, *60*, 123–138.

Ide, S., A. Baltay, and G. C. Beroza (2011), Shallow dynamic overshoot and energetic deep rupture in the 2011 M_w 9.0 Tohoku-Oki earthquake, *Science*, *332*, 1426–1429, doi:10.1126/science.1207020.

Iinuma, T., et al. (2012), Coseismic slip distribution of the 2011 off the Pacific Coast of Tohoku Earthquake (*M*9.0) refined by means of seafloor geodetic data, *J. Geophys. Res.*, *117*, B07409, doi:10.1029/2012JB009186.

Imanishi, K., and W. L. Ellsworth (2006), Source scaling relationships of microearthquakes at Parkfield, CA, determined using the SAFOD pilot hole seismic array, *Geophys. Monogr.*, *170*, 81–90.
Kagan, Y. Y. (1991), 3-D rotation of double-couple earthquake sources, *Geophys. J. Int.*, *106*, 709–716, doi:10.1111/j.1365-246X.1991.tb06343.x.
Kanamori, H. (1977), The energy release in great earthquakes, *J. Geophys. Res.*, *82*, 2981–2987, doi:10.1029/JB082i020p02981.
Kanamori, H., and D. L. Anderson (1975), Theoretical basis of some empirical relations in seismology, *Bull. Seismol. Soc. Am.*, *65*, 1073–1095.
Kiser, E., and M. Ishii (2012), The March 11, 2011 Tohoku-oki earthquake and cascading failure of the plate interface, *Geophys. Res. Lett.*, *39*, L00G25, doi:10.1029/2012GL051170.
Kita, S., T. Okada, A. Hasegawa, J. Nakajima, and T. Matsuzawa (2010), Anomalous deepening of a seismic belt in the upper-plane of the double seismic zone in the Pacific slab beneath the Hokkaido corner: Possible evidence for thermal shielding caused by subducted forearc crust materials, *Earth Planet. Sci. Lett.*, *290*, 415–426, doi:10.1016/j.epsl.2009.12.038.
Koketsu, K., et al. (2011), A unified source model for the 2011 Tohoku earthquake, *Earth Planet. Sci. Lett.*, *310*, 480–487, doi:10.1016/j.epsl.2011.09.009.
Koper, K. D., A. R. Hutko, T. Lay, C. J. Ammon, and H. Kanamori (2011), Frequency-dependent rupture process of the 11 March 2011 M_W 9.0 Tohoku earthquake: Comparison of short-period *P* wave backprojection images and broadband seismic rupture models, *Earth Planets Space*, *63*, 599–602.
Lay, T., C. J. Ammon, H. Kanamori, L. Xue, and M. J. Kim (2011), Possible large near-trench slip during the great 2011 Tohoku (M_w 9.0) earthquake, *Earth Planets Space*, *63*, 687–692, doi:10.5047/eps.2011.05.033.
Lin, W., M. Conin, J. C. Moore, F. M. Chester, Y. Nakamura, J. J. Mori, L. Anderson, E. E. Brodsky, N. Eguchi, and E. Scientists (2013), Stress state in the largest displacement area of the 2011 Tohoku-Oki earthquake, *Science*, *339*, 687–690, doi:10.1126/science.1229379.
Madariaga, R. (1976), Dynamics of an expanding circular fault, *Bull. Seismol. Soc. Am.*, *66*, 639–666.
Maercklin, N., G. Festa, S. Colombelli, and A. Zollo (2012), Twin ruptures grew to build up the giant 2011 Tohoku, Japan, earthquake, *Sci. Rep.*, *2*, doi:10.1038/srep00709.
Marone, C. (1998), Laboratory-derived friction laws and their application to seismic faulting, *Ann. Rev. Earth Planet. Sci.*, *26*, 643–696, doi:10.1146/annurev.earth.26.1.643.
Meng, L., A. Inbal, and J.-P. Ampuero (2011), A window into the complexity of the dynamic rupture of the 2011 M_w 9 Tohoku-Oki earthquake, *Geophys. Res. Lett.*, *38*, L00G07, doi:10.1029/2011GL048118.
Nakajima, J., and A. Hasegawa (2006), Anomalous low-velocity zone and linear alignment of seismicity along it in the subducted Pacific slab beneath Kanto, Japan: Reactivation of subducted fracture zone?, *Geophys. Res. Lett.*, *33*, L16309, doi:10.1029/2006GL026773.
Nakajima, J., F. Hirose, and A. Hasegawa (2009), Seismotectonics beneath the Tokyo metropolitan area, Japan: Effect of slab-slab contact and overlap on seismicity, *J. Geophys. Res.*, *114*, B08309, doi:10.1029/2008JB006101.
Nanjo, K. Z., N. Hirata, K. Obara, and K. Kasahara (2012), Decade-scale decrease in *b* value prior to the *M*9-class 2011 Tohoku and 2004 Sumatra quakes, *Geophys. Res. Lett.*, *39*, L20304, doi:10.1029/2012GL052997.
Okada, Y., K. Kasahara, S. Hori, K. Obara, S. Sekiguchi, H. Fujiwara, and A. Yamamoto (2004), Recent progress of seismic observation networks in Japan—Hi-net, F-net, K-NET and KiK-net, *Earth Planets Space*, *56*, xv–xxviii.
Oth, A. (2013), On the characteristics of earthquake stress release variations in Japan, *Earth Planet. Sci. Lett.*, *377*, 132–141, doi:10.1016/j.epsl.2013.06.037.
Ozawa, S., T. Nishimura, H. Suito, T. Kobayashi, M. Tobita, and T. Imakiire (2011), Coseismic and postseismic slip of the 2011 magnitude-9 Tohoku-Oki earthquake, *Nature*, *475*, 373–376, doi:10.1038/nature10227.
Pulido, N., and L. A. Dalguer (2009), Estimation of the high-frequency radiation of the 2000 Tottori (Japan) earthquake based on a dynamic model of fault rupture: Application to the strong ground motion simulation, *Bull. Seismol. Soc. Am.*, *99*, 2305–2322, doi:10.1785/0120080165.
Roten, D., H. Miyake, and K. Koketsu (2012), A Rayleigh wave back-projection method applied to the 2011 Tohoku earthquake, *Geophys. Res. Lett.*, *39*, L02302, doi:10.1029/2011GL050183.
Shao, G., X. Li, C. Ji, and T. Maeda (2011), Focal mechanism and slip history of the 2011 M_w 9.1 off the Pacific coast of Tohoku Earthquake, constrained with teleseismic body and surface waves, *Earth Planets Space*, *63*, 559–564, doi:10.5047/eps.2011.06.028.
Shearer, P. M., G. A. Prieto, and E. Hauksson (2006), Comprehensive analysis of earthquake source spectra in Southern California, *J. Geophys. Res.*, *111*, B06303, doi:10.1029/2005JB003979.
Simons, M., et al. (2011), The 2011 magnitude 9.0 Tohoku-oki earthquake: Mosaicking the megathrust from seconds to centuries, *Science*, *332*, 1421–1425, doi:10.1126/science.1206731.
Spudich, P., and L. N. Frazer (1984), Use of ray theory to calculate high-frequency radiation from earthquake sources having spatially variable rupture velocity and stress drop, *Bull. Seismol. Soc. Am.*, *74*, 2061–2082.
Suzuki, W., S. Aoi, H. Sekiguchi, and T. Kunugi (2011), Rupture process of the 2011 Tohoku-Oki mega-thrust earthquake (*M*9.0) inverted from strong-motion data, *Geophys. Res. Lett.*, *38*, L00G16, doi:10.1029/2011GL049136.
Takahashi, T. (2012), Three-dimensional attenuation structure of intrinsic absorption and wide-angle scattering of *S* waves in northeastern Japan, *Geophys. J. Int.*, *189*, 1667–1680, doi:10.1111/j.1365-246X.2012.05438.x.
Tsumura, N., S. Matsumoto, S. Horiuchi, and A. Hasegawa (2000), Three-dimensional attenuation structure beneath the northeastern Japan arc estimated from spectra of small earthquakes, *Tectonophysics*, *319*, 241–260, doi:10.1016/S0040-1951(99)00297-8.
Uchida, N., and T. Matsuzawa (2011), Coupling coefficient, hierarchical structure, and earthquake cycle for the source area of the 2011 off the Pacific coast of Tohoku earthquake inferred from small repeating earthquake data, *Earth Planets Space*, *63*, 675–679.
Uchida, N., and T. Matsuzawa (2013), Pre- and postseismic slow slip surrounding the 2011 Tohoku-oki earthquake rupture, *Earth Planet. Sci. Lett.*, *374*, 81–91, doi:10.1016/j.epsl.2013.05.021.
Uchida, N., T. Matsuzawa, W. L. Ellsworth, K. Imanishi, K. Shimamura, and A. Hasegawa (2012), Source parameters of microearthquakes on an interplate asperity off Kamaishi, NE Japan over two earthquake cycles, *Geophys. J. Int.*, *189*, 999–1014, doi:10.1111/j.1365-246X.2012.05377.x.
Uchide, T. (2013), High-speed rupture in the first 20 s of the 2011 Tohoku earthquake, Japan, *Geophys. Res. Lett.*, *40*, 2993–2997, doi:10.1002/grl.50634.
Uchide, T., H. Yao, and P. M. Shearer (2013), Spatio-temporal distribution of fault slip and high-frequency radiation of the 2010 El Mayor-Cucapah, Mexico earthquake, *J. Geophys. Res. Solid Earth*, *118*, 1546–1555, doi:10.1002/jgrb.50144.
Ujiie, K., et al. (2013), Low coseismic shear stress on the Tohoku-Oki megathrust determined from laboratory experiments, *Science*, *342*, 1211–1214, doi:10.1126/science.1243485.
Wang, D., and J. Mori (2011), Frequency-dependent energy radiation and fault coupling for the 2010 M_w8.8 Maule, Chile, and 2011 M_w9.0 Tohoku, Japan, earthquakes, *Geophys. Res. Lett.*, *38*, L22308, doi:10.1029/2011GL049652.

Wessel, P., and W. H. F. Smith (1991), Free software helps map and display data, *Eos Trans. AGU*, *72*, 441.
Yagi, Y., and Y. Fukahata (2011), Rupture process of the 2011 Tohoku-oki earthquake and absolute elastic strain release, *Geophys. Res. Lett.*, *38*, L19307, doi:10.1029/2011GL048701.
Yamada, T., P. G. Okubo, and C. J. Wolfe (2010), Kīholo Bay, Hawai'i, earthquake sequence of 2006: Relationship of the main shock slip with locations and source parameters of aftershocks, *J. Geophys. Res.*, *115*, B08304, doi:10.1029/2009JB006657.
Yamashita, T., T. Okada, T. Matsuzawa, and A. Hasegawa (2004), Scaling law of earthquakes along the plate boundary east off northeastern Japan [in Japanese], *Zisin2*, *56*, 457–469.
Yao, H., P. Gerstoft, P. M. Shearer, and C. Mecklenbräuker (2011), Compressive sensing of the Tohoku-oki M_w 9.0 earthquake: Frequency-dependent rupture modes, *Geophys. Res. Lett.*, *38*, L20310, doi:10.1029/2011GL049223.
Yao, H., P. M. Shearer, and P. Gerstoft (2012), Subevent location and rupture imaging using iterative backprojection for the 2011 Tohoku M_w 9.0 earthquake, *Geophys. J. Int.*, *190*, 1152–1168, doi:10.1111/j.1365-246X.2012.05541.x.
Ye, L., T. Lay, and H. Kanamori (2012), The Sanriku-Oki low-seismicity region on the northern margin of the great 2011 Tohoku-Oki earthquake rupture, *J. Geophys. Res.*, *117*, B02305, doi:10.1029/2011JB008847.
Ye, L., T. Lay, and H. Kanamori (2013), Ground shaking and seismic source spectra for large earthquakes around the megathrust fault offshore of Northeastern Honshu, Japan, *Bull. Seismol. Soc. Am.*, *103*, 1221–1241, doi:10.1785/0120120115.
Zhao, D., A. Hasegawa, and S. Horiuchi (1992), Tomographic imaging of *P* and *S* wave velocity structure beneath northeastern Japan, *J. Geophys. Res.*, *97*, 19,909–19,928, doi:10.1029/92JB00603.
Zhao, D., Z. Huang, N. Umino, A. Hasegawa, and H. Kanamori (2011), Structural heterogeneity in the megathrust zone and mechanism of the 2011 Tohoku-oki earthquake (M_w 9.0), *Geophys. Res. Lett.*, *38*, L17308, doi:10.1029/2011GL048408.